ChemComm

COMMUNICATION

View Article Online
View Journal | View Issue

Published on 23 October 2013. Downloaded by University of Tennessee at Knoxville on 10/06/2016 22:39:43.

Cite this: *Chem. Commun.*, 2014, **50**, 201

Received 26th September 2013,
Accepted 22nd October 2013

DOI: 10.1039/c3cc47377e

www.rsc.org/chemcomm

One-pot synthesis of size- and morphology-controlled 1-D iron oxide nanochains with manipulated magnetic properties†

Qingliang He,[ab] Tingting Yuan,[a] Xingru Yan,[ab] Zhiping Luo,[c] Neel Haldolaarachchige,[d] David P. Young,[d] Suying Wei*[ab] and Zhanhu Guo*[a]

Polypropylene grafted maleic anhydride (PP-MA, 2500 g mole^{-1}) has demonstrated its unique capability to synthesize 1-D ferromagnetic hard (292.7 Oe) γ-Fe_2O_3 nanochains made of ~24 nm nanoparticles *vs.* PP-MA with 8000 g mole^{-1} for the synthesis of 1-D ferromagnetic soft (70.5 Oe) γ-Fe_2O_3 nanochains (30 nm) made of flowerlike nanoparticles.

Self-assembly of 1-dimensional (1-D) hierarchical nanostructures with magnetic colloidal nanoparticles (NPs) as building blocks represents a powerful versatile bottom-up method to obtain multi-functional nano-materials with unique properties.[1–5] The inherent magnetic dipole–dipole interactions and the van der Waals forces of the ferromagnetic NPs are usually the driving forces to enable the self-assembly construction at the nano-scale.[3,6,7]

Though the assembly of well-defined 1-D iron (oxide) nano-chains has been reported,[8–11] the imperative hard template aided or magnetic field induced assembly is time consuming and costly in most cases. Recently, we have successfully used a plastic additive – polypropylene grafted with two maleic anhydride (PP-*g*-MA, structure shown in ESI,† Scheme S1), to synthesize mono-dispersed hollow hematite colloidal NPs[12] through a facile bottom up method.[12–16] In addition, without an external magnetic field, the self-assembled 1-D maghemite (γ-Fe_2O_3) nanochains consisting of spherical NP building blocks with very high coercivity (H_c, 518 Oe) were achieved by simply lowering the PP-*g*-MA concentration.[12] However, it is impossible to tune the building block structures of the obtained nanochains by varying the PP-*g*-MA concentration. Several other PP-*g*-MAs (chemical structures shown in Scheme S2, ESI†) have been studied; however, none of them has shown the capability to manipulate the morphology of the obtained Fe_2O_3 NPs (transmission electron microscopy, TEM images shown in the right column of Scheme S2, ESI†). To the best of our knowledge, simultaneous control of the self-assembled final morphologies and the starting building block configurations of 1-D nanochains with manipulated magnetic properties *via* bottom up colloidal synthesis (even by using powerful surfactants like fatty acids) remains a major challenge.

Herein, we report a unique function of PP grafted with terminal maleic anhydride (denoted as "PP-MA" to distinguish from PP-*g*-MA, structure shown in Scheme S3, ESI†) to synthesize 1-D γ-Fe_2O_3 nanochains with tunable chain diameters, building-block structures, and magnetic properties through a one-pot bottom up method. By only varying the molecular weight (M_n) of PP-MA while maintaining its concentration and the same reaction conditions, ferromagnetic hard γ-Fe_2O_3 nanochains (diameter: ~24.0 nm and coercivity: 292.7 Oe) consisting of well-defined single spherical NPs as building blocks were synthesized using PP-MA ($M_n \approx 2500$); while ferromagnetic soft hierarchical γ-Fe_2O_3 nanochains (diameter: ~30.0 nm and coercivity: 70.5 Oe) were self-assembled from flower-like NP building blocks using PP-MA ($M_n \approx 8000$). This is the first report on controlling the building block structure, self-assembly morphology and magnetic properties of the well-defined 1-D γ-Fe_2O_3 nanochains in a facile one-pot bottom-up approach at the gram-level yield.

Through thermal-decomposition of 3.50 g $Fe(CO)_5$ in 100 mL xylene solution containing 0.25 g PP-MA ($M_n \approx 8000$), the formation of 1-D nanochains (diameter: ~30.0 nm) was observed in the TEM image, Fig. 1a. The enlarged TEM image in Fig. 1b demonstrates that the building blocks of these nanochains are consisted of unique flower-shape NPs, which are totally different from the nanochains with single NP building blocks reported in previous work.[12] Selected area electron diffraction (SAED) patterns and lattice spacing in the high resolution TEM (HRTEM) image (Fig. S1, ESI†) confirm the sole existence of γ-Fe_2O_3 in the nano-chains.[17] The self-assembled 1-D nanochains can be realized *via* replacing PP-MA ($M_n \approx 8000$) with PP-MA ($M_n \approx 2500$). When 0.25 g PP-MA ($M_n \approx 2500$) was used in decomposing 3.50 g $Fe(CO)_5$ in 100 mL xylene, the formed colloidal NPs were observed to assemble into 1-D nanochains consisting of quasi-spherical NPs instead of the flower shape NP building blocks, when drop-cast on the carbon coated copper TEM grid, the average

[a] *Integrated Composites Laboratory (ICL), Dan F. Smith Department of Chemical Engineering, Lamar University, Beaumont, Texas 77710, USA. E-mail: zhanhu.guo@lamar.edu; Tel: +1 409 880 7654*
[b] *Department of Chemistry and Biochemistry, Lamar University, Beaumont, Texas 77710, USA. E-mail: suying.wei@lamar.edu; Tel: +1 409 880 7976*
[c] *Department of Chemistry and Physics, Fayetteville State University, Fayetteville, NC 28301, USA*
[d] *Department of Physics and Astronomy, Louisiana State University, Baton Rouge, Louisiana 70803, USA*

† Electronic supplementary information (ESI) available: Experimental details and additional information including TEM, SEM, SAED, *etc.* See DOI: 10.1039/c3cc47377e

Published on 23 October 2013. Downloaded by University of Tennessee at Knoxville on 10/06/2016 22:39:43.

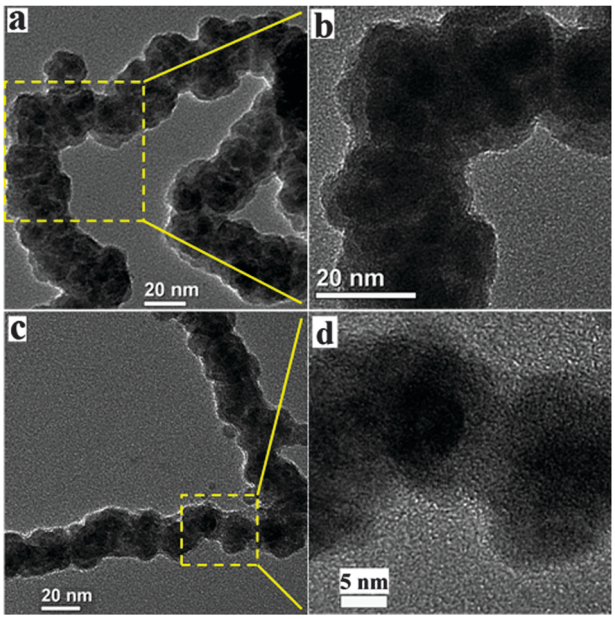

Fig. 1 TEM images of γ-Fe_2O_3 nanochains obtained from thermal-decomposition of 3.50 g $Fe(CO)_5$ in 100 mL xylene with (a and b) 0.25 g PP-MA ($M_n \approx 8000$); and (c and d) 0.25 g PP-MA ($M_n \approx 2500$). Average chain diameter is: (a and b) ~30.0 nm, and (c and d) ~24.0 nm, respectively.

diameter was ~24.0 nm, Fig. 1c and d. SAED patterns and lattice spacing in the HRTEM image (Fig. S2, ESI†) also indicate the sole existence of γ-Fe_2O_3. X-ray photoelectron spectroscopy (XPS, Fig. S3, ESI†) further confirms that both two nano-chains are in pure γ-Fe_2O_3 form without any sign of impurity. Scanning electron microscopy (SEM) images (Fig. 2a and b) further demonstrate highly entangled curvy nanochains with diameters of ~24.0 and ~30.0 nm synthesized from different M_n PP-MA, indicating that both γ-Fe_2O_3 nanochains remain intact during the formation of nanocomposites from drying the colloids.

The different chain morphologies are caused by the difference in capping strength from different M_n PP-MA on the magnetic NPs. The MA group in PP-MA can be tightly chemisorbed onto the magnetic NPs[12] similar to the carboxylic acid surfactant.[18] Larger M_n PP-MA (*i.e.*, $M_n \approx 8000$) resulted in low MA density in the reaction system, and a lower capping strength on the surface of magnetic NPs was thus observed. At low concentrations, for example, 0.25 g PP-MA ($M_n \approx 8000$), the aggregation of small magnetic clusters led to the formation of flower-shape NPs grown from the highly concentrated nuclei upon thermal-decomposition of $Fe(CO)_5$.[2,19] The further assembly of these flower "aggregates" is driven by the balance between attractive forces (magnetic dipolar attractions, and van der Waals forces)[20] and the steric hindrance from the coordinating PP-MA backbones. When lower M_n PP-MA was used in the same amount, only individual NPs can be formed because of tighter capping strength and more condense PP-MA backbones will bound on the surface of the obtained NPs. The curvy chain assembly is the demonstration of well-defined head-to-tail NP arrangement, in which the strong attractive magnetic dipolar forces overcome the repulsive forces from PP-MA backbones. Meanwhile, the density of PP-MA adsorbing on the obtained NPs can also be increased upon increasing the PP-MA concentration; hence, enhanced repulsive forces against these magnetically attractive NPs

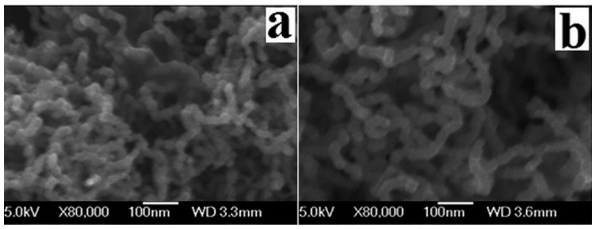

Fig. 2 SEM images of γ-Fe_2O_3 nanochains stabilized by PP-MA with M_n of (a) 2500, and (b) 8000. Composition: 3.50 g $Fe(CO)_5$ in 100 mL xylene with 0.25 g PP-MA. Average chain diameter is: (a) ~24.0 and (b) ~30.0 nm.

can be achieved while maintaining all other reaction parameters. In this case, the disassembly of the nano-chain structure with separated magnetic NPs could be realized, also different morphologies will be achieved with different concentrations of PP-MA.

Upon increasing the concentration of PP-MA ($M_n \approx 8000$) from 0.25 to 0.50 g in thermal-decomposition of 3.50 g $Fe(CO)_5$ in 100 mL xylene, partially assembled nanochains (Fig. S4a, ESI†) and partially separated flower-shape NPs ("intermediate") comprising of 3-leaf (marked in triangle area) and 4-leaf (marked in square) shape "aggregates" were observed, Fig. 3a. The SAED patterns confirm that these NPs were also pure γ-Fe_2O_3, Fig. S4b (ESI†). This "intermediate" other than the 1-D nanochain was also clearly observed by SEM, Fig. S5 (ESI†). When using 0.50 g PP-MA ($M_n \approx 2500$) in decomposing 3.50 g $Fe(CO)_5$ in 100 mL xylene, mono-dispersed core–shell NPs were observed, Fig. 3b. Strong rings in SAED patterns (Fig. S6a, ESI†) correspond to (311), (400) and (440) planes of γ-Fe_2O_3 (PDF#39-1346);[17] and (104) and (300) planes of α-Fe_2O_3 (PDF#33-0664). The HRTEM image (Fig. S6b, ESI†) clearly demonstrates the core–shell structure, and a shell lattice fridge of the α-Fe_2O_3 (300) plane with a spacing of 1.45 Å. This suggests that a γ-Fe_2O_3 core–α-Fe_2O_3 shell structure was formed with stronger capping strength from PP-MA ($M_n \approx 2500$). Upon the generation and growth of small nuclei from thermal-decomposition of $Fe(CO)_5$, iron colloidal NPs coordinated by PP-MA were not chemically stable under ambient conditions and oxidation took place on these particle surfaces and were converted to γ-Fe_2O_3.[12] While maintaining the same PP-MA concentration during the synthesis, decreasing the M_n of PP-MA from 8000 to 2500 obviously resulted in an increase of the MA coordinating density. Therefore, the more stable α-Fe_2O_3 shell[21] formed on the surface of the γ-Fe_2O_3 core is probably due to the

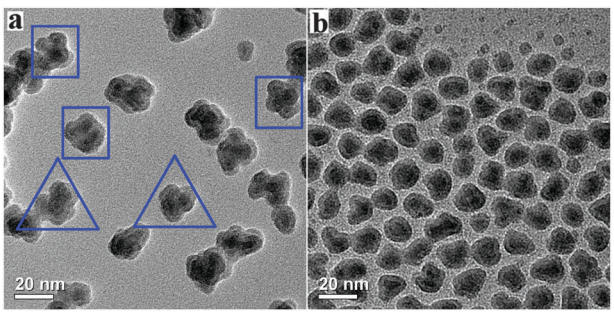

Fig. 3 TEM images of (a) flower-shape and (b) quasi-spherical Fe_2O_3 nanoparticles from thermal-decomposition of 3.5 g $Fe(CO)_5$ in 100 mL xylene with (a) 0.5 g PP-MA ($M_n \approx 8000$); and (b) 0.50 g PP-MA ($M_n \approx 2500$). Average particle size is: (a) ~19.4 nm, and (b) ~14.1 nm.

 This journal is © The Royal Society of Chemistry 2014

Published on 23 October 2013. Downloaded by University of Tennessee at Knoxville on 10/06/2016 22:39:43.

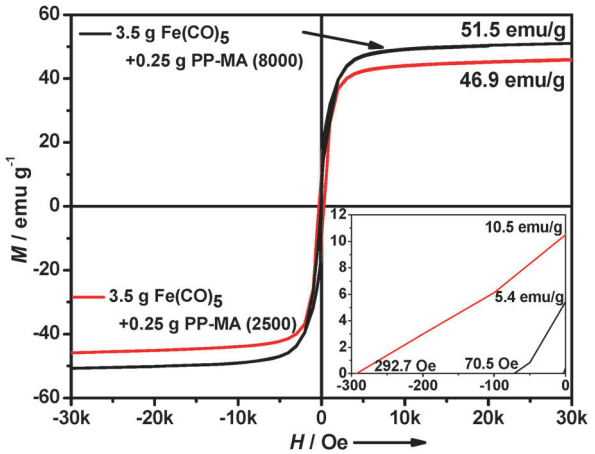

Fig. 4 Room temperature magnetic hysteresis loops of the 1-D γ-Fe_2O_3 nanochains stabilized by two M_n PP-MAs (2500 *vs.* 8000).

tighter capping strength on the surface of these NPs, which is similar to the surface disorder of γ-Fe_2O_3.[22] These observations clearly demonstrate the capability of PP-MA in synthesizing stable magnetic Fe_2O_3 NPs with tunable particle size, composition, shape and self-assembly morphology. Changing the PP-MA molecular weights in turn controls the balance of the overall net force between the attractive and repulsive forces, which is believed to intrigue these aforementioned differences. Scheme S4 (ESI†) depicts the proposed mechanisms in detail.

Besides these unique morphological evolution observations, different magnetic properties were also observed. Materials with coercivity (H_c) greater than 200 Oe are defined as ferromagnetic hard; while those with H_c smaller than 200 Oe are defined as ferromagnetic soft.[23,24] Room temperature magnetic properties reveal that the γ-Fe_2O_3 nanochains (30 nm in diameter) have higher saturation magnetization (M_s) than γ-Fe_2O_3 nanochains (24 nm in diameter), Fig. 4. More importantly, the H_c of 30 nm γ-Fe_2O_3 nanochains is about 70.5 Oe, reflecting a ferromagnetic soft material; while the H_c of 24 nm γ-Fe_2O_3 nanochains is 292.7 Oe, corresponding to a ferromagnetic hard material. It can be concluded that the magnetic properties such as coercivity (ferromagnetic soft *vs.* hard) of thus synthesized 1-D nanochains can be easily controlled by only changing the molecular weight of PP-MA. Comparing the as-synthesized 24 nm diameter 1-D γ-Fe_2O_3 nanochains (Fig. 1c) with their 30 nm counterpart (Fig. 1a), it is found that the smaller diameter nanochain structure led to a higher aspect ratio, in which the further resulting higher shape anisotropy is responsible for the observed higher H_c.[25] In addition, the smaller size and dimensionality of the 24 nm γ-Fe_2O_3 nanochains than their 30 nm counterparts, Fig. 1 and 2, may also change the magnetization reversal mechanism.[26] This mechanism may also contribute to the further enlarged H_c for the smaller diameter ($\sim$24 nm) 1-D γ-Fe_2O_3 nanochains. Meanwhile, the sharply decreased H_c of the $\sim$30 nm γ-Fe_2O_3 nanochains is also in good agreement with the size dependent coercivity, in which the larger diameter building block NPs can significantly decrease the coercivity.[27] Details regarding these magnetic properties are provided in ESI.† For the "intermediate"-flower shape NPs and the core–shell NPs (Fig. 3), the room temperature magnetic property results (Fig. S7, ESI†) reveal a much lower saturation magnetization (M_s, 9.3 emu g^{-1}) for the core–shell NPs formed in PP-MA ($M_n \approx 2500$) than the flower shape γ-Fe_2O_3 NPs formed in PP-MA ($M_n \approx 8000$), which also confirmed the existence of the antiferromagnetic α-Fe_2O_3 shell.

In summary, we have demonstrated an extremely facile one-pot bottom up approach to synthesize well defined 1-D γ-Fe_2O_3 nanochains with easily controlled building block configurations (single *vs.* flower shape NPs), self-assembly morphologies towards the further manipulation of magnetic properties (ferromagnetic soft *vs.* hard). PP-MA with appropriate MA grafting density and reaction concentration is of key importance to achieve these evolved different 1-D γ-Fe_2O_3 nanochains. The merits of this colloidal synthesis approach including gram-level production and mild conditions can be used for the self-assembly of other 1-D magnetic nanomaterials with tailored magnetic properties for a variety of applications such as high-density magnetic storage, sensors and environmental remediation.[28]

This work was supported by the Seeded Research Enhancement Grant (REG) of Lamar University and NSF CMMI 10-30755 to perform TGA and DSC. DPY acknowledges support from the NSF under grant DMR-1306392.

References

1 L. He, M. Wang, J. Ge and Y. Yin, *Acc. Chem. Res.*, 2012, **45**, 1431.
2 M.-R. Gao, S.-R. Zhang, J. Jiang, Y.-R. Zheng, D.-Q. Tao and S.-H. Yu, *J. Mater. Chem.*, 2011, **21**, 16888.
3 P. Y. Keng, I. Shim, B. D. Korth, J. F. Douglas and J. Pyun, *ACS Nano*, 2007, **1**, 279.
4 B. D. Korth, P. Keng, I. Shim, S. E. Bowles, C. Tang, T. Kowalewski, K. W. Nebesny and J. Pyun, *J. Am. Chem. Soc.*, 2006, **128**, 6562.
5 N. Zheng, X. Bu, H. Lu, L. Chen and P. Feng, *J. Am. Chem. Soc.*, 2005, **127**, 14990.
6 J. Gao, B. Zhang, X. Zhang and B. Xu, *Angew. Chem., Int. Ed.*, 2006, **45**, 1220.
7 Y. Lalatonne, J. Richardi and M. Pileni, *Nat. Mater.*, 2004, **3**, 121.
8 P. Wang, H. Jaganathan and A. Ivanisevic, *Small*, 2011, **7**, 202.
9 H. Wang, Q. Chen, Y. Yu and K. Cheng, *Dalton Trans.*, 2011, **40**, 4810.
10 J. Gong, S. Li, D. Zhang, X. Zhang, C. Liu and Z. Tong, *Chem. Commun.*, 2010, **46**, 3514.
11 F. Zhang and C. C. Wang, *J. Phys. Chem. C*, 2008, **112**, 15151.
12 Q. He, T. Yuan, S. Wei, N. Haldolaarachchige, Z. Luo, D. P. Young, A. Khasanov and Z. Guo, *Angew. Chem., Int. Ed.*, 2012, **51**, 8842.
13 (*a*) W. Lu, J. Fang, K. Stokes and J. Lin, *J. Am. Chem. Soc.*, 2004, **126**, 11798; (*b*) Z. Guo, L. Henry, V. Palshin and E. Podlaha, *J. Mater. Chem.*, 2006, **16**, 1772.
14 J. Zhang, A. Kumbhar, J. He, N. Das, K. Yang, J. Wang, H. Wang, K. L. Stokes and J. Fang, *J. Am. Chem. Soc.*, 2008, **130**, 15203.
15 Z. Quan, Y. Wang, I.-T. Bae, W. S. Loc, C. Wang, Z. Wang and J. Fang, *Nano Lett.*, 2011, **11**, 5531.
16 Y. Xu, Y. Qin, S. Palchoudhury and Y. Bao, *Langmuir*, 2011, **27**, 8990.
17 X. Gu, Z. Sun, S. Wu, W. Qi, H. Wang, X. Xu and D. Su, *Chem. Commun.*, 2013, **49**, 10088.
18 S. Sun and C. Murray, *J. Appl. Phys.*, 1999, **85**, 4325.
19 S. Palchoudhury, Y. Xu, A. Rushdi, R. A. Holler and Y. Bao, *Chem. Commun.*, 2012, **48**, 10499.
20 V. Puntes, K. Krishnan and A. Alivisatos, *Science*, 2001, **291**, 2115.
21 L. Machala, J. Tuček and R. Zbořil, *Chem. Mater.*, 2011, **23**, 3255.
22 A. Millan, A. Urtizberea, N. Silva, F. Palacio, V. Amaral, E. Snoeck and V. Serin, *J. Magn. Magn. Mater.*, 2007, **312**, L5.
23 Q. He, T. Yuan, J. Zhu, Z. Luo, N. Haldolaarachchige, L. Sun, A. Khasanov, Y. Li, D. Young, S. Wei and Z. Guo, *Polymer*, 2012, **53**, 3642.
24 Q. He, T. Yuan, Z. Luo, N. Haldolaarachchige, D. P. Young, S. Wei and Z. Guo, *Chem. Commun.*, 2013, **49**, 2679.
25 P. M. Rao and X. Zheng, *Nano Lett.*, 2011, **11**, 2390.
26 B. Y. Geng, J. Z. Ma, X. W. Liu, Q. B. Du, M. G. Kong and L. D. Zhang, *Appl. Phys. Lett.*, 2007, **90**, 043120.
27 D. Leslie-Pelecky and R. Rieke, *Chem. Mater.*, 1996, **8**, 1770.
28 (*a*) S. Singamaneni, V. N. Bliznyuk, C. Binek and E. Y. Tsymbal, *J. Mater. Chem.*, 2011, **21**, 16819; (*b*) S. Wei, Q. Wang, J. Zhu, L. Sun, H. Lin and Z. Guo, *Nanoscale*, 2011, **3**, 4474.